Chapter 10

An Overview of Principles and Designs of Hydraulic Fracturing Experiments and an Inquiry into the Influence of Rock Permeability and Strength on Failure Mode

Kenneth Imo-Imo Eshiet and Yong Sheng

Additional information is available at the end of the chapter

http://dx.doi.org/10.5772/intechopen.69732

Abstract

The relevance of hydraulic fracturing experiments in the analysis of subsurface flow mechanisms and interactions during fracking operations underpins past and current efforts towards designing and implementing more representative physical models. An overview has been presented that comprehensively discusses the key elements and design requirements for successful experimentations. In setting up a hydraulic fracturing experiment, it is imperative that, in line with the research objective, the physical model that includes the initial and boundary conditions, wellbore configuration, type of fracturing fluid and injection rate be a true representative of actual reservoir/underground flow environments. This investigation recognises the main elements that form the framework for effective laboratory scale experiments, which comprise the specimen, *in-situ* stresses, pore pressure, fluid injection, duration, and visualisation and monitoring. Furthermore, an examination of the influence of rock properties on the characteristics of fracturing and failure of rocks subjected to wellbore conditions indicates a trend highly dependent on rock strength and permeability. Soft and highly permeable rocks tend to cause an inward collapse of the wellbore cavity. Cavity size is also shown to have a considerable effect on the failure process. Wellbore stability is inversely related to cavity size; larger cavities are found to be less stable.

Keywords: hydraulic fracturing experiment, fracture propagation, fracturing behaviour, rock failure, subsurface, reservoir, rocks, fluid pressure

1. Introduction

The versatility and importance of hydraulic fracturing is easily shown in the range of its applications. The technique is applied in the estimation of *in-situ* stress [1, 2], the exploitation

of geothermal energy [3], enhanced oil and gas recovery (EOR) operations [4], enhanced coal bed methane (ECBM) operations [5, 6], shale gas production [7–9] and the control of the structure and deformation of rock roof during coal mining [10].

The use of hydraulic fracture experiments is an age-long approach applied to understand mechanical interactions between fluids and solid materials. These experiments have proven to be invaluable and have been instrumental in providing insights into the various mechanisms that take place due to the co-existence of fluids and intact solid materials. Until recently, hydraulic fracturing experiments in tandem with fluid observations were the major means of investigating the mechanisms of flow within porous media. The advent and rapid advancement of computational capability as well as reductions in cost have paved the way for the pervasive use of numerical and analytical methods. These methods, just like in any other field of study, have moved the frontier of research by providing a means were forecasting tools can be more easily developed. The general limitations of numerical/analytical techniques lie in the fact that the input data, initial and boundary conditions have to be a true representation of conditions that are modelled. An erroneous or misapplied condition will definitely lead to false results. Numerical methods also often require constitutive equations/models, which must be accurately formulated and applied. The enormous advantages are only derived through thorough verification and validation exercises. Field observations and laboratory experiments are veritable sources of information that can serve as both input data and means of comparison with actual or pseudo-actual events. Field information is usually scarce and expensive to obtain. They are site-specific and may not be suitable for different geographical locations. Physical models in laboratories are therefore crucial and are increasingly relied upon; they are used to

- make up for the lapses in numerical/analytical models, for instance, by providing further evidence or support regarding certain processes not indicated,
- provide input data for numerical/analytical models and
- verify and validate numerical/analytical models.

A comprehensive and critical examination of hydraulic fracturing experiments used to explore subsurface flow mechanisms is presented. This embodies a detailed depiction of the design and conduct of experimental set-ups meant to assess the role of well and reservoir conditions on mechanisms of fracturing and well collapse. This forms the backdrop for a full description of a case study encompassing the set-up, execution and implication of a typical hydraulic fracturing experiment used in simulating the weakening and disintegration of rocks subjected to pressurised conditions. This is illustrated in Section 3.

2. Overview of hydraulic fracturing experiments: composition and design considerations

2.1. Specimen

The underlying purpose of hydraulic fracturing experiments is to imitate real-life field scale conditions. Therefore, the initial, boundary and prevailing conditions should replicate the

http://dx.doi.org/10.5772/intechopen.69732

field environment, even though as a miniature version. Key parameters to consider include *in-situ* stresses, overburden stresses, pore pressure, pore pressure gradient, drawdown, injection pressure, injection velocity, fluid properties, etc. Creating an environment with the right combination of these parameters requires placing the specimen in an enclosure subjected to the target condition. Sample materials are either synthesised artificially or cored from natural rocks.

Artificial rock materials are made in various ways. In the form of cement mortar, they have been derived from a 1:1 mixture of cement and fine siliceous sand or cement and quartz sand using a material to water ratio of 40% (2:5) [10–13] or from Portland cement mixed with water at a ratio of 40% (2:5) [14, 15]. A mixture of cement, quartz sand and gravel can also be made and have been used by Zhao et al. [11] to create materials with glutenite-like characteristics (**Figure 1**). These are the main constituents of glutenite hydrocarbon reservoirs, which consist of air tight low permeability rocks ranging, for instance, between 0.015 and 0.3 mD [16]. This type of rock requires stimulation by hydraulic fracturing to instigate a yield of economic value. A characteristic constituent of glutenite rocks is gravel. These have a controlling effect on the effectiveness of the stimulation process since they affect the geometry and propagation of hydraulic fractures [11]. Thermoplastics such as polymethyl methacrylate (PMMA) [1–3] are used as alternative artificial specimen materials [17]. PMMA is a transparent homogeneous glass-like material. Its physical properties are documented and its strengths are comparable with those of rock. They are easily moulded and their transparency aids visualisation of strain and fracture marks. Finally, as will be discussed later, it is possible to make synthetic specimens from glass beads bonded by epoxy resin. Further notes on this are given in Section 3.

In order to imitate naturally fractured rocks, it is possible to instil or cause the generation of fractures during the creation of artificial rock specimens. Hydrostone, which has properties similar to rock, can be used to systematically create pre-existing fractures with predefined dimensions and inclinations. It is a gypsum product composed mainly of plaster and cement. It sets easily and is suitable where joints or fracture planes are to be created during

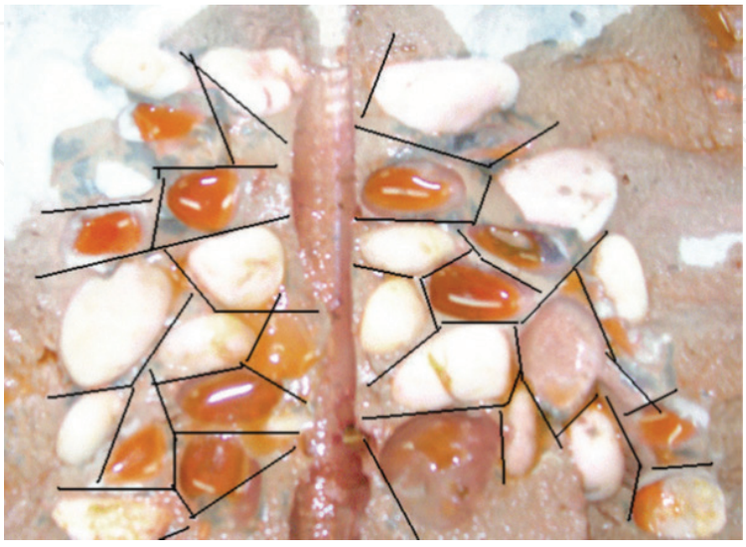

Figure 1. Glutenite showing fracture outlines in black [11].

casting [18]. Pre-fractures can also be created by placing different kinds of paper sheet into blocks during casting [12]. The papers may vary in material property, thickness or inclination, reflecting the characteristics of real life pre-fractures. Another way of generating pre-fractures is by heating moulded specimens [13, 14]. This is achieved by placing them in an oven for a specific period after curing. For instance, in the work of de Pater and Beugelsdijk [14], samples were heated at a temperature of 200°C for 2 weeks, and in the work of Zhou et al. [13], samples were heated at a constant temperature of 400°C for 3 hours. As the specimen dehydrates, random fractures are developed due to shrinkage which may be comparable to discontinuities in real rocks.

Natural rock samples such as shale, limestone, sandstone, rhyolite, granite, etc., may be cut from boulders at quarries (e.g. [18]), outcrops (e.g. [19, 20]) or mining sites (e.g. [21]). A comparison of hydraulic fracturing mechanisms on assorted types of natural rocks is presented, for example, in the work of Zoback et al. [22], Matsunaga et al. [23] and Brenne et al. [24]. The following sets of rocks were compared: Ruhr sandstone, Weber sandstone and a South African gabbro [22]; coarse-grained Inada granite, fine-grained Akiyoshi marble and Komatsu andesite [23]; and marble, limestone, sandstone, andesite and rhyolite [24].

Soil specimens are likewise used in hydraulic fracturing experiments, where the fracture morphology, conditions governing the fracturing process and fracture mechanisms are to be investigated. Whereas hydraulic fracturing in soils is not well reported, comprehensive studies were carried out by Murdoch [25–27], Ito et al. [28] and Omori et al. [29] on samples of clay and sand. Murdoch's work highlighted the dependency of the fracturing mechanism on soil water content.

2.2. *In-situ* stresses

It is imperative to ensure that the sample is under the influence of stress states similar to natural reservoir conditions. To achieve this, the sample is subjected to external stresses applied either in 2D for a biaxial condition or 3D for a triaxial condition. *In-situ* stresses are usually exerted along the outer boundary of specimens and is applied and monitored through a servo-controlled system. The hydraulic voltage stabiliser can be used to apply *in-situ* stresses [10] on specimens, which have to be initially placed in a biaxial or triaxial set-up. As a rule of thumb, *in-situ* stresses should be applied prior to the introduction of hydraulic fluids.

The state of stress can be established through a loading frame powered directly by a hydraulic system [10] or the loading frame may consist of hydraulic pump powered flat jacks, which regulate the pressure on the external surfaces [18, 23]. A triaxial pressure machine equipped with pistons can also be used [11, 12, 14, 15] (**Figure 2**). To simulate a desired stress condition, the specimen is placed between pressurised pistons with platens furnished with flat spherical/square sheets for even distribution of pressure. To prevent the generation of shear stresses, a Teflon sheet smeared with lubricant is placed between the specimen and the platen. *In-situ* stresses have been exerted by positioning the specimen in a chamber lined with neoprene bladders [25]. When the bladders are inflated with air, pressure is then applied on the specimen through the bladder.

http://dx.doi.org/10.5772/intechopen.69732

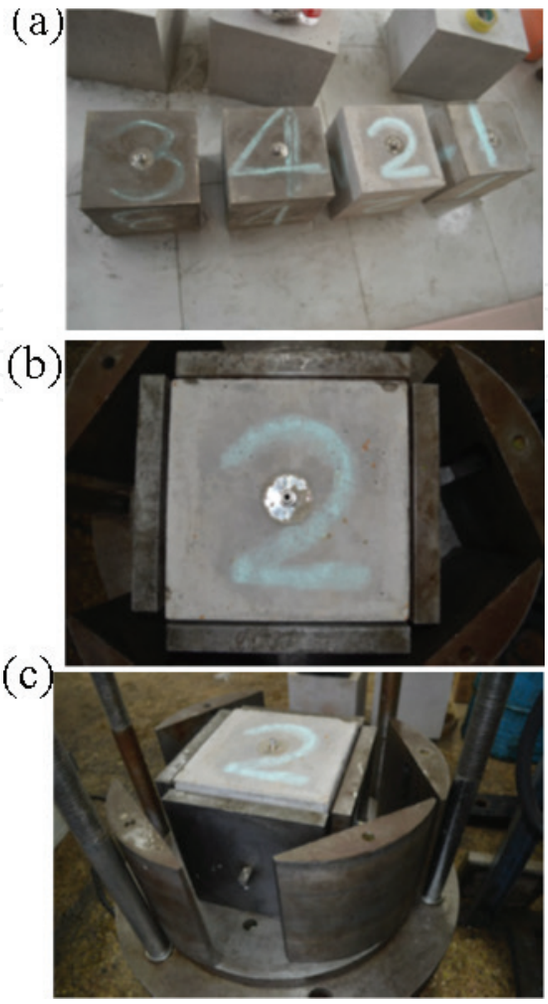

Figure 2. Cubic specimen preparation and application of 3D *in-situ* stresses [10]. (a) Specimen under curing. (b) Applying *in-situ* stress in triaxial assembly: plan view. (c) Applying *in-situ* stress in triaxial assembly: side view.

Where hydraulic fracturing experiments are conducted in a cylindrical core holder or triaxial cell, *in-situ* stresses are created by applying circumferential confining pressures and axial loads [20, 24]. In Liberman [20], confining pressure is applied on the specimen through rubber sleeves placed between the core specimen and the encasing cylinder. As the pressure between the rubber sleeve and cylinder is increased, the same is transferred via the sleeves, which grips the sample. In the same assembly, an axially and vertically mounted piston simulates the overburden stress through downward movements. The Hoek triaxial cell is an example of a cylindrical chamber and is made up of a hollow steel cylinder with threaded detachable ends. It is conventionally used to determine the triaxial strength of drill cores and is equipped to induce confining and axial stresses, which makes it suitable for hydraulic fracturing experiments (e.g. [24]).

In essence, specimens are shaped in either cylindrical or cubic (block) forms, even though more variety of stress systems can be applied on block shapes. If the direction of the principal stresses is altered, it is then possible to simulate different tectonic stress regimes on cubic

samples [12, 15]. A normal faulting regime is where the major principal stress is vertical (S_V) such that $S_V > S_H > S_h$., where S_V is the vertical stress, S_H is the maximum horizontal stress and S_h is the minimum horizontal stress. A strike-slip faulting regime occurs when the major principal stress is horizontal in the order $S_H > S_V > S_h$. In the reverse (Thrust) faulting regime, the stress field becomes compressive, the major principal stress is in the lateral direction and each horizontal stress is individually greater than the vertical stress, i.e. $S_H > S_h > S_V$ [30, 31]. The influence of horizontal stress differential on fracturing process is investigated by Blanton [18].

2.3. Pore pressure

As shown by Murdoch [25], it is possible to measure the pore pressure of samples while enclosed in the fracturing chamber; however, pore pressure is often not explicitly represented. Samples may be fully saturated, partially saturated or completely unsaturated. For convenience, after curing, samples are initially fully saturated or totally dried. For saturated samples, the axial and confining pressure generates the 'total' stress, which is the sum of the pore pressure and effective stress. If the sample is dry, the pore pressure is nil, so the total stress is equivalent to the effective stress. In simulating the fluid pressure within fractures, the concept of the 'net pressure' is adopted. This is the driving pressure, which influences, to a large extent, the fracture dilation and growth pattern. The driving pressure, P_d, is given as

$$P_d = P_f - S_3 \tag{1}$$

Where P_f is the pore pressure of the fracture and S_3 is the minimum principal stress. The pore pressure of the fracture must be greater than the minimum principal stress ($P_f > S_3$) for dilation and fracture propagation to occur. For natural fractures, the stress normal to the fracture plane may not necessarily be the minimum principal stress [12]. S_3 may then be substituted with the stress component perpendicular to the fracture plane, S_n. Thus, by employing these relationships, pore pressure in fractures and the material matrix is implicitly accounted for; nonetheless, this precludes the *in-situ* pore pressure gradient and drawdown that define the spatially variable pore conditions in the lateral and vertical directions.

2.4. Fluid injection

Water is the most common type of fluid used for hydraulic fracturing and is usually mixed with a variety of chemical additives depending on the characteristic of fluid mixture desired. Additives may serve all or any combination of several purposes including the following: friction reduction (e.g. slickwater), thickening (e.g. Guar beans), prevention of microorganism growth and biofouling (biocides), oxygen removal to check corrosion of pipes and the removal of damages caused by drilling mud (acids). The primary function of fracturing fluids is to create fractures as well as convey proppants that are placed within the fractures. Silica sand, as a natural material, is normally used as a proppant. Artificial proppants are alternative options and could be in the form of ceramic beads, prepared from sintered bauxite, or metal (aluminium) beads.

http://dx.doi.org/10.5772/intechopen.69732

For hydraulic fracturing experiments, attempts are made to use fluids with similar characteristics as those employed in field scale operations. Water-based fluids are used, with guar gum being the only additive, to modify the viscosity of the fracturing fluid [10, 12, 13]. In other instances, where the original property of water is to be maintained, it is purified by distillation [24] or deionisation [21] to ensure it is demineralised. To study the effect of fluid properties (e.g. viscosity), other types of fluids such as oil and drilling mud [20, 22, 23] and glycerine [25] may be used to induce fracturing. Glycerine is a viscous liquid that dissolves in water.

The inclusion of proppants in fracturing fluids in any form is rarely practiced in hydraulic fracturing experiments. Proppants keep the initiated fractures open as the fluid flows between the fracture planes. They are, thus, designed to have sufficient strength in order to keep the fractures open after the injected fluid pressure is released. Propped fractures increase the permeability of the reservoir rock; however, the relevance of the functionality of proppants has not been considered as an essential subject of investigation in laboratory hydraulic fracturing experiments.

It is imperative that the fracturing fluids are mixed with tracers so as to easily mark the pattern of fractures. The tracer may be a fluorescent powder as used in the works of Wang et al. [19], de Pater and Beugelsdijk [14] and Beugelsdijk et al. [15]; or a dye, as applied by Zhao et al. [11] and Murdoch [25].

The fracturing fluid injected through the borehole is controlled in terms of either fluid velocity/discharge or fluid pressure. The target magnitude of fluid pressure or flow rate is a function of several factors. The pressure or flow rate must be sufficient to initiate and propagate fractures and is usually supplied by a servo-controlled pumping system (e.g. [10, 11, 13, 19, 22, 24]). Wang et al. [19] applied constant flow rates from as low as 1e−6 m^3/s to as high as 1.67e−4 m^3/s on shale samples having Young's modulus and compressive strength up to 48,610 and 407 MPa, respectively, while in the work of Deng et al. [10], constant injection pressures reaching ≈ 30 MPa were used to propagate fractures in synthetic samples made from cement mortar. Blanton [18] employed a *pressure intensifier* to introduce the fracturing fluid at a constant flow rate of 8.194e−7 m^3/s (0.05 cu in/s) in order to induce fractures on Devonian shale and hydrostone samples. A positive displacement pump was used by Beugelsdijk et al. [15] to apply an array of flow rates into cement mortar samples; the results obtained were then compared against observations from a base injection flow rate of 8.3e−9 m^3/s. A similar pumping procedure on cement mortar was implemented by Zhou et al. [13] and Zhou et al. [12] to build-up a maximum injection fluid pressure of 19.28 and 140 MPa, respectively, by injecting fracturing fluid at a constant rate of 4.2e−9 m^3/s. A range of flow rates between 8.33e−4 m^3/s (5 mL/min) and 4.17e−3 m^3/s (25 mL/min), generating up to a maximum fracture pressure of ≈ 70 MPa was applied by Alpern et al. [17] on PMMA specimens.

There is no standardised fracturing flow rate or pressure. Certain key considerations determine the selection of injection flow regimes. These include material strength, fluid property (e.g. viscosity), *in-situ* stresses, boundary conditions, pore pressure, pre-existing fractures, wellbore orientation, reservoir/underground flow conditions, pre-existing fluids (e.g. oil, gas, water), phenomena to be examined, objectives of the investigation, etc. A cross-section of injection flow rates and pressures adopted in various hydraulic fracturing experiments is presented in **Table 1**.

Reference	Injection flow rate	Injection pressure	Sample material	Duration
Zoback et al. [22]	–	1e−4 to 3 MN/m^2/s	Natural rocks: sandstone & Gabbro	≈100 s
Zoback et al. [22]	2.64e−9 to 6.6e−7 m^3/s	9.6e-2 to 17.1 MN/m^2/s	Natural rocks: sandstone & gabbro	≈140 s
Murdoch [25]	3.3e−8 m^3/s	–	Silty clay soil	≈400 s
Liberman [20]	8.3e−7 m^3/s	–	Dolomite & sandstone	≈60–530 s
Liberman [20]	8.3e−8 m^3/s	–	Concrete	≈2500–3750 s
Alpern et al. [17]	8.3e-8 to 4.17e-7 m3/s	–	PMMA	–
Brenne et al. [24]	1.0e−7 m^3/s	–	Natural rocks: Marble, Limestone, Sandstone, Andesite, Rhyolite	≈50–200 s
Matsunaga et al. [23]	6.67e−8 m^3/s	–	Acrylic resin; natural rocks: Marble & Granite	≈200 s
Molenda et al. [32]	1.0e−7 m^3/s	0.3 MN/m^2/s (until 105 MN/m^2)	Natural rocks: Rhyolite & Sandstone	≈400–800 s
Beugelsdijk et al. [15]	8.3e−9 m^3/s	–	Portland cement	≈6500–15,500 s
Blanton [18]	8.194e-7 m^3/s	–	Hydrostone; natural rocks: Shale	≈230 s
Zhou et al. [13]	4.2e-9 m^3/s	Up to 19.28 MN/m^2	Cement mortar	≈1600 s
Zhou et al. [12]	4.2e−9 m^3/s	Up to 140 MN/m^2	Cement mortar	–
Wang et al. [19]	1e−6 to 1.67e−4 m^3/s	Up to 69 MN/m	Natural rock: shale, coal & sandstone	≈900–5000 s

Table 1. Fracturing fluid injection pressure and flow rates used in hydraulic fracturing experiments.

2.5. Duration

Sufficient time must be allowed for fracture initiation and proliferation. The duration of individual tests vary and usually depends on the extent of fracturing that has occurred. Progression in fracturing can be reliably monitored through the evolution in fluid pressure. The breakdown pressure is an indication that fracturing has taken place and the beginning of the decline of pressure built up during fluid injection. The test is continued until the decay in pressure reaches a stable magnitude. Advancement in fracturing is influenced by the material type, fracturing fluid injection flow rate/pressure rate, fracturing fluid viscosity, amongst other factors. The time interval for a complete cycle ranges from as low as 50 s (e.g. [24]) to more than 15,500 s (e.g. [15]).

The rate of fluid infiltration into rock is determined by the fluid viscosity, the rock permeability and porosity. Pressure build-up is controlled by the fluid injection flow rate and wellbore storage, and the time scale is influenced by the fluid injection flow rate and viscosity [14]. Because of the variability in viscosities of the different fracturing fluids adopted for hydraulic fracturing experiments, the product of the fluid injection rate and its viscosity ($q-\mu$ value)

http://dx.doi.org/10.5772/intechopen.69732

is sometimes preferred as a more reliable parameter to control pressurisation and fracture geometry [15]. This product has a direct impact on the time scale. The $q-\mu$ parameter permits a clearer interpretation of interrelationships between fracturing fluid flow rate, viscosity and fracture geometry. A standardisation of the correlation between these parameters may then be possible.

3. Case study: hydraulic fracturing experiments with natural and synthetic rocks

Laboratory fracturing experiments are often used to monitor the deterioration and disintegration of rocks under prescribed and controlled simulated sub-surface reservoir conditions. Tests were conducted on series of synthetic and natural rock samples subjected to differing operating and boundary conditions. Artificial samples were made, first, using glass beads bonded together with diluted epoxy resin to imitate soft permeable rocks low in strength; second, using luting cement and; last, with calcium sulphate hydrate (gypsum plaster). Limestone was used as natural samples. The early and non-progressive collapse of the low strength and highly permeable synthetic rocks (bonded glass bead materials) illustrates the combined effects of permeability and strength on the failure mode. This effect is further highlighted during tests on natural rocks possessing relatively lower permeability and higher strength. Observed occurrences during the tests show the role of prevailing/operating well and reservoir conditions as well as the physical and mechanical properties of materials on mechanisms that result in collapse failure.

3.1. Experimental set-up and methodology

Experiments were mainly conducted at Wolfson Multiphase Flow Laboratory, School of Earth and Environment, University of Leeds.

3.1.1. Sample preparation and design

Three sets of samples were used consisting of natural rock specimens and artificially prepared (synthetic) specimens. The artificial specimens include materials made from glass beads bonded by epoxy resin diluted with acetone. Specimens were also made from samples of luting cement and calcium sulphate hydrate (gypsum plaster). Natural rock (limestone) samples were sourced from Tadcaster, North Yorkshire, United Kingdom.

The synthetic glass specimens were prepared using graded glass beads between 640 and 760 μm in diameter (**Figures 3** and **5**). In order to create adhesion between the particles, an epoxy resin was applied. In addition to its bonding properties, epoxy resins possess good quality mechanical properties when left to cure, especially in terms of tensile strength and stiffness. They also have good chemical and thermal properties and are waterproof or at least resistant to water penetration. Its high stiffness and low permeability may sometimes compromise the properties of the bonded assembly, particularly where relatively high permeability, high porosity and low

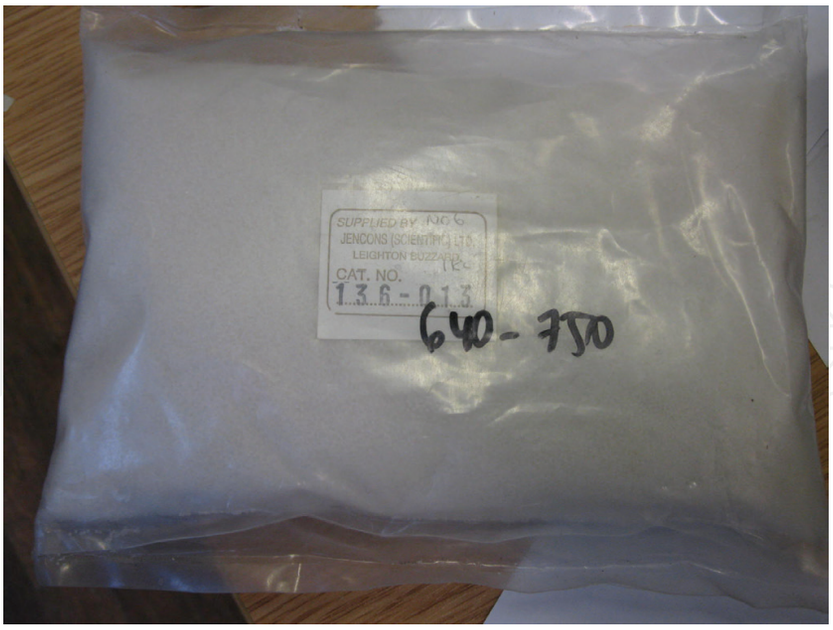

Figure 3. Graded glass beads a range of diameter between 640 and 750 μm.

stiffness is to be preserved. To attenuate this effect, the epoxy resin was diluted with acetone in order to prolong the setting period as well as to reduce the stiffness, at the same time increasing its permeability to desirable magnitudes. A second set of artificial specimens consisted of luting cement powder, which was set by mixing it with water. Limestone was used as an exemplification of natural rock.

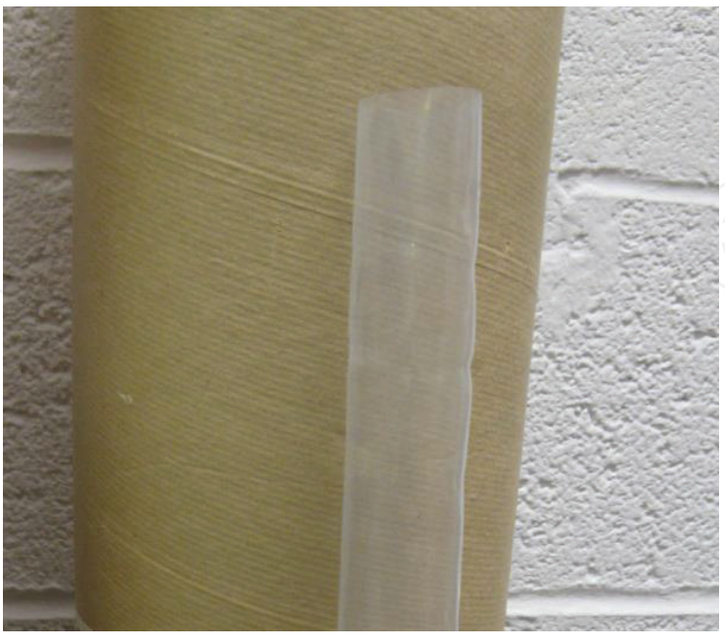

Figure 4. Flexible transparent plastic tubing used to cast glass beads.

http://dx.doi.org/10.5772/intechopen.69732

Figure 5. Preparation of synthetic rock samples (glass beads bonded with epoxy resins). (a) View 1 and (b) View 2.

To replicate the moisture content condition typical of reservoir rocks, all the specimens were fully saturated. They were fully immersed in water and placed in a vacuum chamber connected to a vacuum pump and operated for several hours to enable the removal of trapped air within the material. The glass samples were casted using flexible lightweight plastic tubes (**Figures 4** and **5**) with additional tubing placed at the centre to make it hollow. The diameter of the plastic tube is 37 mm, implying that the outer diameter of the samples were the same. An inner diameter of 10 mm was created. **Figures 5** and **6** illustrate part of the casting procedure and the final dry glass specimens before saturation (**Figures 7** and **8**).

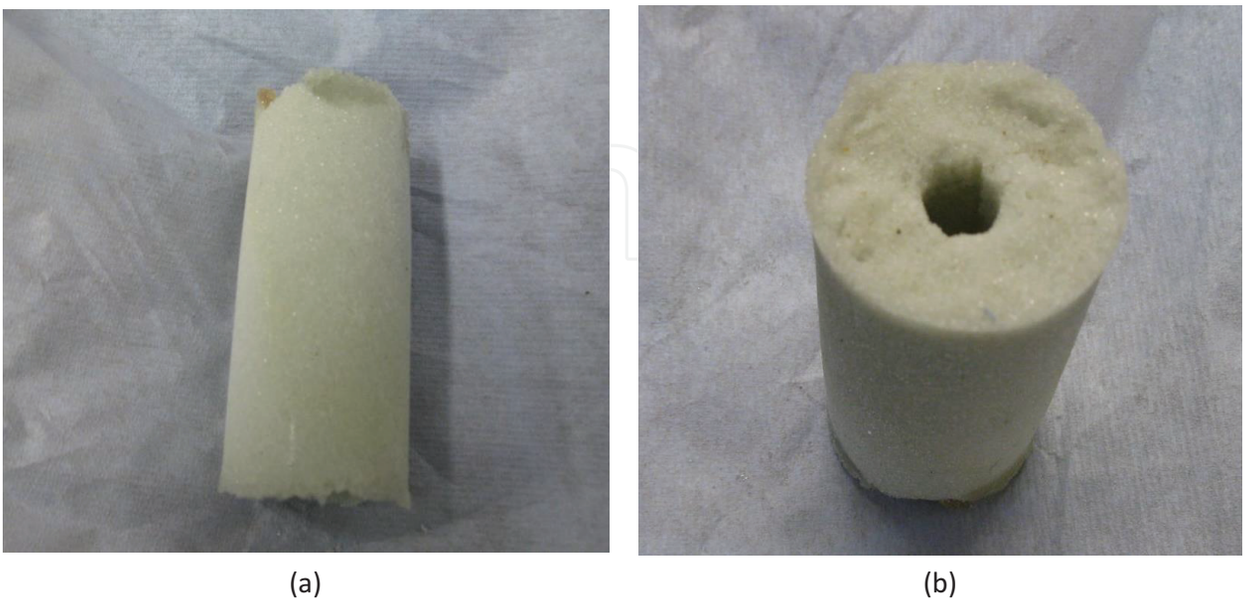

Figure 6. (a) A longitudinal view and (b) an oblique view of the synthetic rock (bonded glass beads).

Figure 7. An immersed synthetic rock (luting cement), soaked in water before placement in the vacuum chamber.

Figure 8. The saturation process and removal of trapped air using a vacuum chamber and pump.

http://dx.doi.org/10.5772/intechopen.69732

3.1.2. Equipment requirement and set-up

3.1.2.1. Equipment requirement for fracture tests

A comprehensive list of the main equipment utilised at various stages of the experiment are as follows:

- **Auxiliary equipment:** These include moulds (used to produce casts of synthetic specimens), beakers, test tubes, spatulas, vacuum pumps and vacuum chambers.
  - ***Specification of vacuum pump***

    Model type: MZ 20NT

    Serial Number: 34810908

    Maximum capacity: 2.3/2.5 m^3/h

    4.0 mbar

- **Equipment for fracture tests:**
  - ***Fracturing cell***

Type: Triaxial 2-probe resistivity core holder

Specification:

Serial number: CL-T-RES-1.5x6-5K-109

Maximum pressure: 5000 Psi

Material: aluminium

Manufacturer: Phoenix Instruments, USA

  - ***CT scanner***

    Manufacturer: PICKER

    Model number: PQ-2000

    Supplied by: Core Lab Instruments, USA

    Resolution: (250 × 250 × 1000) μm

  - ***Hydraulic hand pumps***: to carry out preliminary hydraulic fracturing tests, especially where real time and continuous monitoring is not required.

    Type and specification:

    Type: ENERPAC P141

    Maximum capacity: 10,000 Psi/700 bars

- **Computing:** A set of computers (at least two) to monitor and control test operations, as well as to process the scan images. Computers are also required during material testing.

- **Fracturing fluids:**
  - Shell Thermia Oil (for exerting the confining pressure)
  - Distilled water (for exerting the internal pressure)

3.1.3. Experimental set-up and test procedure

A cell was used comprising a standard triaxial resistivity core holder (**Figure 9**), with a core diameter = 38 mm. The sample sizes were made to fit the core. The inlet and outlet plugs of the cell were linked to a network consisting of two hydraulic pumps (**Figure 10**): an inlet pump that drives and regulates the injection fluid at the prescribed flow rate and pressure through the hollow (internal hole) of the specimen when seated within the core holder and another pump to drive a continuous flow of fluid around the circumference of the specimen within the core, which also exerts a regulated confining pressure. A continuous flow of distilled water was injected through the internal hole of the hollow specimen, while a continuous stream of Shell Thermia Oil was allowed to flow around the circumference of the specimen. The outer fluid pressure was applied via rubber sleeves placed in direct contact with the specimen, with the fluid flowing between the rubber sleeves and the metal core casing, creating a mechanical

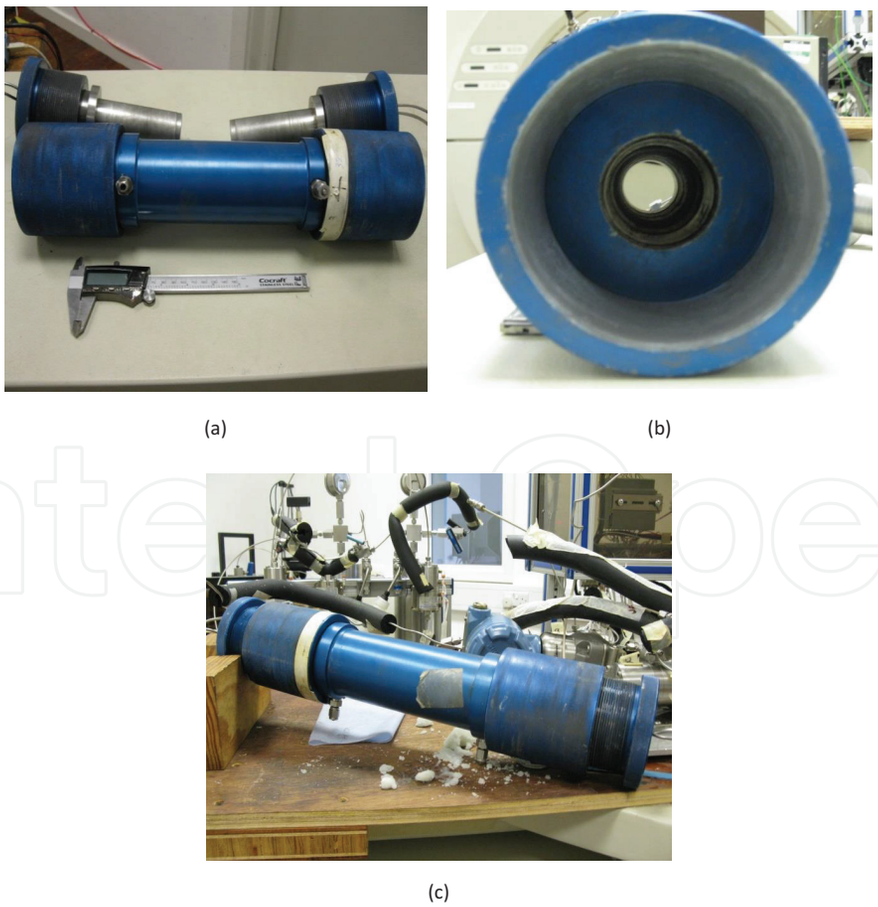

Figure 9. (a) Components of the triaxial core holder, (b) the cross-section showing the hole where specimens are placed, and (c) the coupled triaxial core holder.

http://dx.doi.org/10.5772/intechopen.69732

circumferential pressure. The control and monitoring of the internal and external fluid flow rates and pressures was performed using a computer.

To facilitate the real time and continuous monitoring of the deformation and fracturing processes within the specimen, the triaxial core holder was placed in a CT scanning machine (**Figure 11**). Periodic scan images together with records of fluid pressure profiles provide the relevant results and the premise for their interpretation.

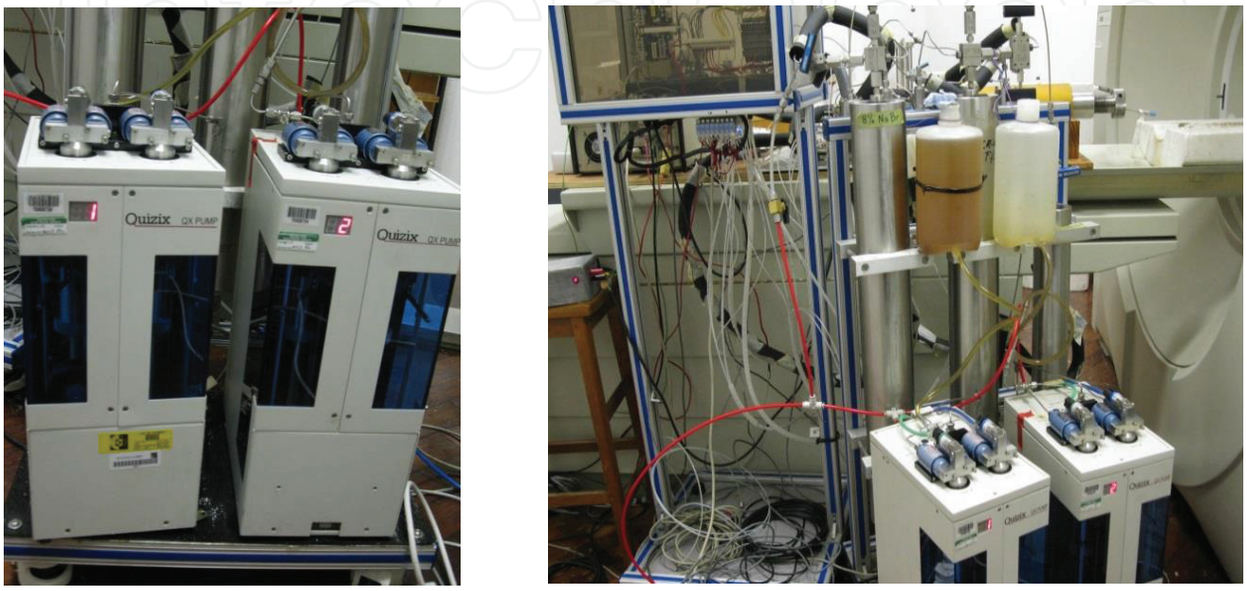

Figure 10. (a) Layout of pumps and (b) position with respect to the CT scanner.

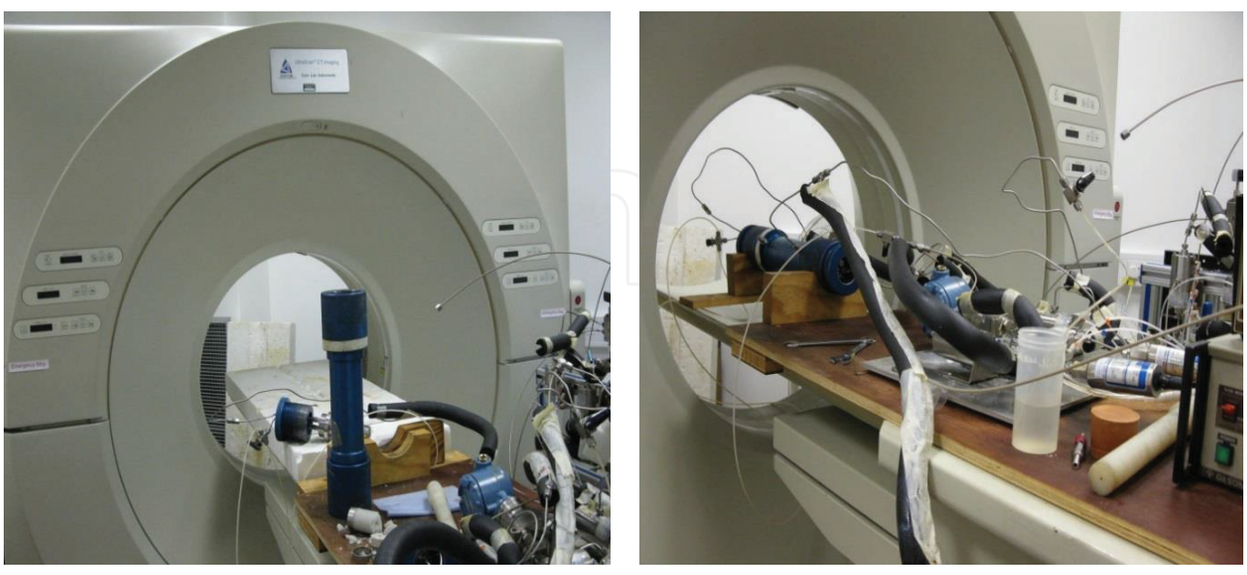

Figure 11. CT scanner (a) before the placement of the core holder and (b) after the core holder is kept in position.

While fluid (Shell Thermia Oil) was pumped through the rubber sleeves to exert an external pressure, an internal pressure was also exerted by pumping fluid (distilled water) through the hollow section of the specimen. Since the inlet ports are not aligned with the centre of the inner hole of the specimen, as shown in **Figure 12**, fluid flow is not restricted to the hollow alone but has the tendency of flowing across the cross-sectional surface area of the specimen. The effect of this is considerably reduced because of the radial and straight grooves that direct the flow to the centre (**Figure 12**). In addition, due to the small sizes of the pores in the specimen in comparison to the size of the hollow, fluid flow through the cross-sectional surface area is considered negligible since it is much smaller than that in the hollow. The maximum output from each pump is 50 ml/min with a single pump consisting of a pair of cylinders.

The synthetic rock specimen (glass beads) was casted to fit the core holder. The dimensions are given as follows: external diameter = 37.8 mm, internal (hollow) diameter = 10 mm and length = 100 mm. The test was conducted under an average temperature of 21°C. There was no axial loading except that exerted by the contact between the top and bottom cross-sectional surfaces of the specimen and the ram tips. The differential stress condition was therefore regarded as being essentially controlled by the confining stress.

3.1.4. Mode of fluid application

For the first batch of tests on the synthetic rock specimens, attempts were made to simultaneously and gradually increase fluid pressure at the hollow and circumferential boundary of the specimen. Starting with an initial fluid pressure of zero, the magnitude was increased in similar increments. The objective was to stabilise the fluid pressure at the inner and outer

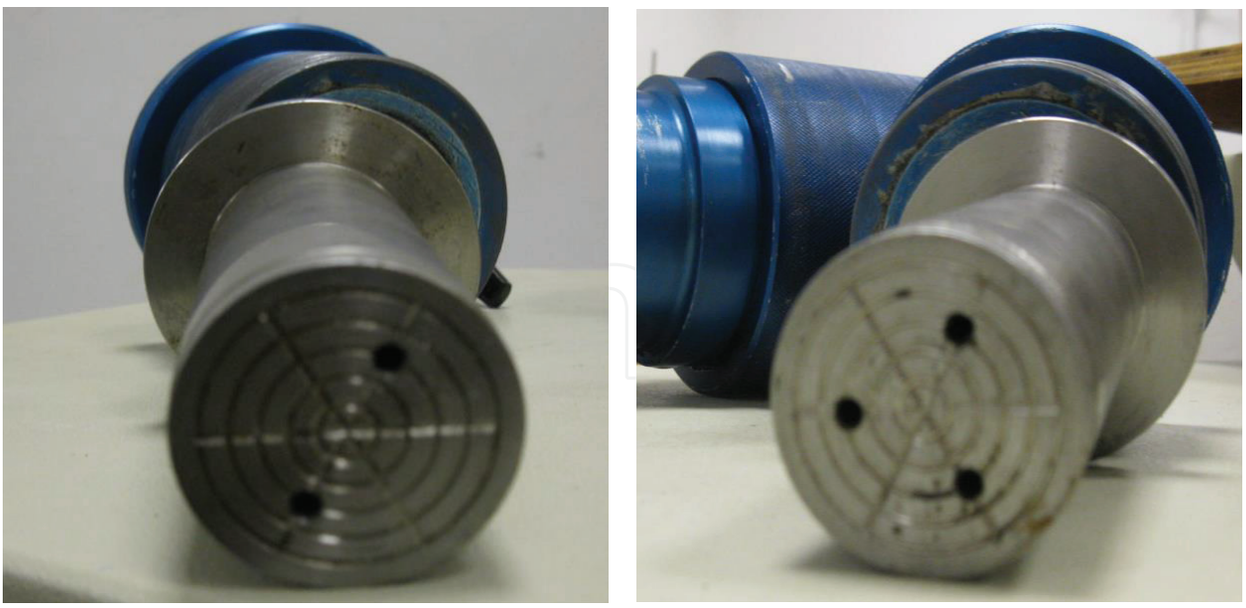

Figure 12. Ram tips showing the inlet ports where fluid is driven into the hollow of the specimen. (a) Tip with two ports, (b) Tip with three ports.

http://dx.doi.org/10.5772/intechopen.69732

radial boundaries at a relatively high magnitude, then maintaining this value at the outer boundary while gradually reducing the fluid pressure at the inner boundary in order to create a correspondingly increasing pressure gradient. By doing this, the maximum pressure occurs at the outer boundary and the minimum pressure at the inner boundary.

For the second batch of tests conducted using samples made from luting cement, the outer boundaries (circumferential and cross-sectional) were kept under atmospheric pressure while fluid was continuously injected through the hollow. The pressure of the injected fluid was gradually increased. The internal hole of the luting cement specimen was deliberately made not to cut through its entire length so as to imitate well bottomhole conditions. A third batch of tests was conducted using samples made from calcium sulphate hydrate (gypsum plaster) with through internal holes. The gypsum specimen was produced by mixing the dry plastic powder with water and allowing it to set (Eq. (2)). The dry gypsum powder is originally formed by heating gypsum at temperatures above 150°C to dehydrate it.

$$2\,CaSO_4 \cdot 4\,H_2O + Heat \rightarrow 2\,CaSO_4 \cdot H_2O + 3\,H_2O \quad (2)$$

The fourth set of tests was conducted on limestone, which included different specimens differentiated by the size of their internal core (7.6 and 21.5 mm). One test was performed on a small hollow specimen (7.6 mm) and the other on a larger hollow specimen (21.5 mm). Fluid pressure was applied by maintaining the internal pressure at zero and then slowly increasing the circumferential pressure until a maximum attainable value was obtained. The internal and external fluid pressure records are provided for the first and fourth batches of tests.

4. Result and discussion

4.1. Tests on synthetic rock samples: bonded glass beads

In order to establish a pressure gradient on the core sample, the internal and external fluid pressures were slowly and steadily increased (**Figure 13**) with the intention of gradually stepping down the internal fluid pressure after a sufficiently stable high pressure value is attained (e.g. 5000 Psi). Three individual sets of test on three different days (Day 1, Day 2 and Day 3) were successfully performed (**Figures 14–17**). The synthetic rock samples were varied according to their inter-particle bond strength and stiffness. Specimens with the lowest values were tested on Day 1. Subsequently, additional specimens were casted. The bond strength and stiffness were increased and the test repeated on Day 2. The test was repeated again on Day 3 after further increase in inter-particle bond strength and stiffness. Since the glass beads were randomly packed, the porosity for all specimens is estimated to be 40%. It is also assumed that their permeability is within the same range. The changes in bond strength and stiffness are achieved by altering the mix ratio between the epoxy resin and acetone. A reduction in the proportion of acetone directly decreases the bond strength as well as the bond stiffness.

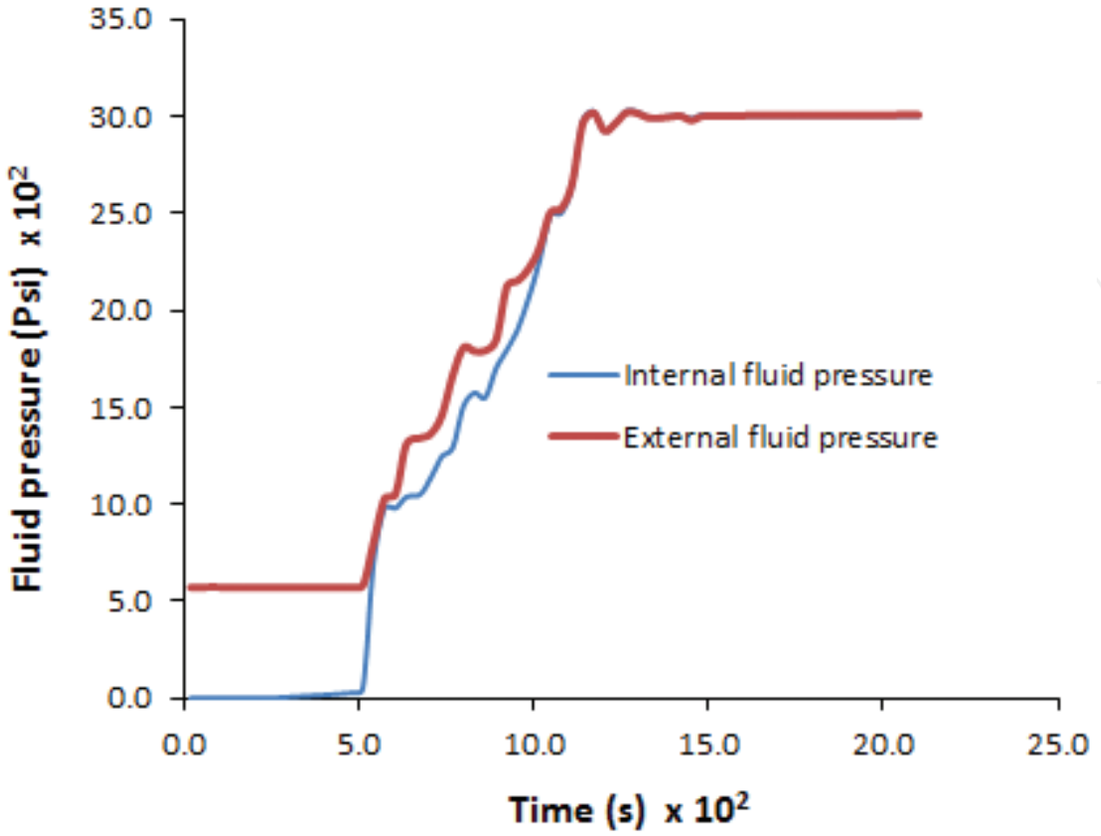

Figure 13. External and internal fluid pressure during injection (strongest sample).

During the incremental administration of fluid pressure, the strength of the synthetic rock material contributes to the magnitude of fluid pressure that can be attained. The strength of the material limits the maximum fluid pressure that can be applied before failure. Results for the weakest specimen (**Figure 14**) show a complete collapse and closure of the internal walls as well as a severe deformation of the external boundaries; this occurred during the application of fluid pressure and the establishment of pressure equilibrium between the internal and external boundaries.

Although fluid pressure was applied simultaneously and in increments, it was impossible to build up pressure beyond a certain threshold, even so, the material was unable to sustain the built-up fluid pressure due to its rapid failure coupled with its high porosity and permeability. Where the strength and stiffness of the material is increased, the maximum allowable build-up pressure increases and the mode of failure differs (**Figures 15** and **17**). Whereas the external circumferential (radial) boundary still remained intact, there was an initial expansion of the inner cavity due to the increasing fluid pressure at this area, which continued until material failure and collapse of the cavity (**Figure 15**). Even when the specimen material strength was further increased, a similar occurrence was observed (**Figure 17**), although the expansion of the cavity has been omitted in the scan images. It is observed that the integrity and form of collapse failure of specimens with similar porosity and permeability are subject to their inter-particle bond strength and stiffness. For such specimens, failure and collapse may occur without the establishment of a pressure gradient. For identification purpose, the levels of bond strength and stiffness are categorised as low, medium and high strength.

http://dx.doi.org/10.5772/intechopen.69732

(a)

(b)

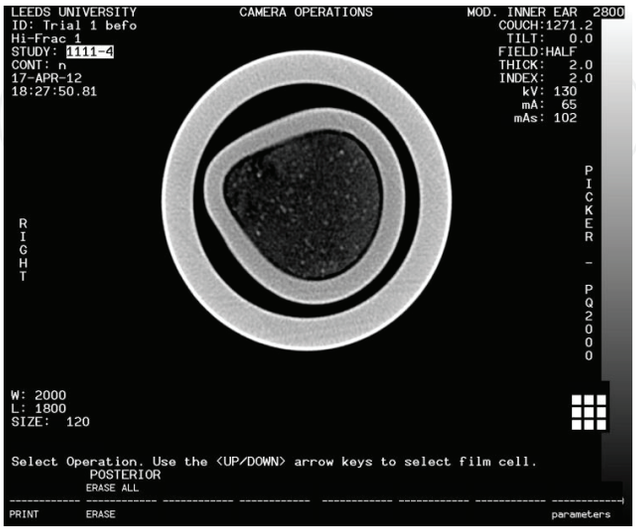

(c)

Figure 14. (a–c) Scan images of the synthetic rock at different times after collapse (low strength).

(a)

(b)

(c)

Figure 15. Scan images of the synthetic rock at different times (a and b) before, and (c) after collapse (medium strength).

http://dx.doi.org/10.5772/intechopen.69732

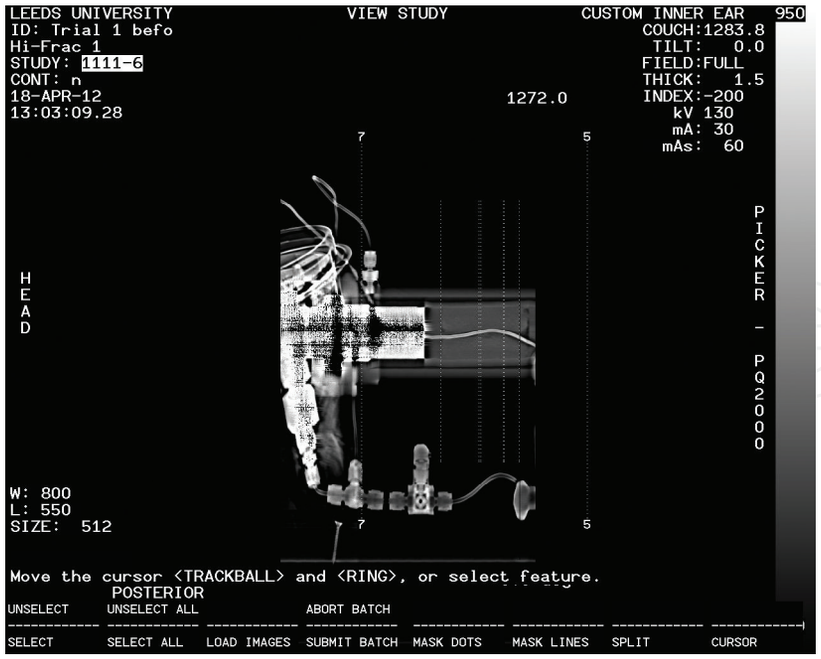

Figure 16. Layout of the core holder containing the synthetic rock specimen.

Figure 17. Scan image of the synthetic rock after collapse (high strength).

4.2. Tests on luting cement samples

The second batch of tests was conducted using luting cement. The configuration of the specimen and mode of fluid flow/fluid pressure application is different. The cavity of the hollow specimen was not extruded through the entire length; rather it was terminated at three quarters of the longitudinal section. Fluid was injected continuously into the cavity at increasing pressures using a manually operated hydraulic hand pump (**Figure 18**). There was no differential

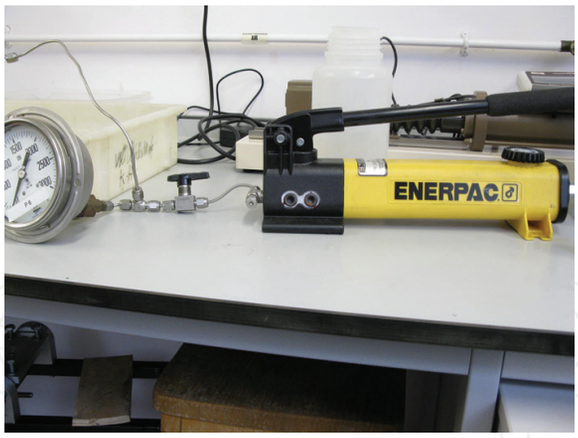

Figure 18. The manually operated hydraulic hand pump.

stress condition as axial and confining loading were not applied. The decision not to apply boundary stress conditions was necessary in order to ascertain the location as well as the mode of initiation and propagation of fractures during injected fluid pressure build-up, in cases where boundary stresses are neglected. *In-situ* and boundary stresses are known to have significant influences on the failure of wells and processes controlling fracturing.

Figure 19 illustrates the failure and fracturing pattern. A single fracture initiates at the bottom of the cavity and propagates with an orientation perpendicular to the cavity, which eventually splits the specimen. The mode of fracturing indicates the preferred location of initiation, direction and orientation of fractures in the absence of principal stress conditions. It was not necessary to obtain scan images.

4.3. Tests on gypsum plaster samples

A similar test was conducted on specimens made from calcium sulphate hydrate (gypsum plaster). Whereas the mode of application of fluid flow/pressure and the boundary stress conditions were the same as the second batch of tests, the cavity was drilled through the entire length of the specimen (analogous to specimens used for the first batch of tests). **Figure 20** shows the set-up of the tests, also carried out without utilising a core holder. An automated hydraulic pump (**Figure 10**) instead of a manually operated hand pump was used. The ends

Figure 19. Luting cement specimen showing failure and horizontal fracturing at the bottomhole. (a) Longitudinal view, (b) Cross-sectional view.

http://dx.doi.org/10.5772/intechopen.69732

Figure 20. Experimental set-up showing the injection of fluid through a gypsum plaster specimen.

of the specimen were sealed with improvised plugs; however, persistent leakages through the ends of the specimen prevented sufficient build-up of fluid pressure during fluid injection. Placing the specimen in a core holder could be a viable solution, although the effect of boundary stresses may not be totally eliminated.

The final set of tests was conducted on a natural rock (limestone) involving two specimens with different cavity sizes. The specimens used in the first and second tests had cavity diameters of 7.9 and 21.5 mm, respectively (**Figures 21–23**). Their external diameters were the same, given as 37.8 mm. For both tests, the internal and external fluid pressures were raised to about 3000 Psi (20.68 MPa) and then the internal fluid pressure slowly reduced while the fluid pressure at the outer circumferential boundary was kept constant. The smaller cavity specimen was still intact even after the internal pressure was effectively reduced to about 2000 Psi

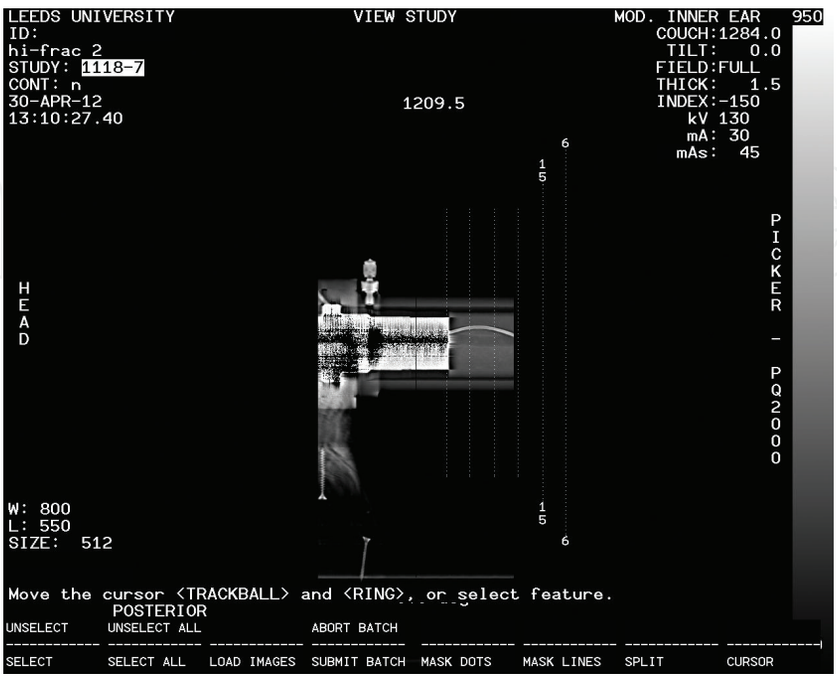

Figure 21. Longitudinal layout of the core holder containing the limestone specimen.

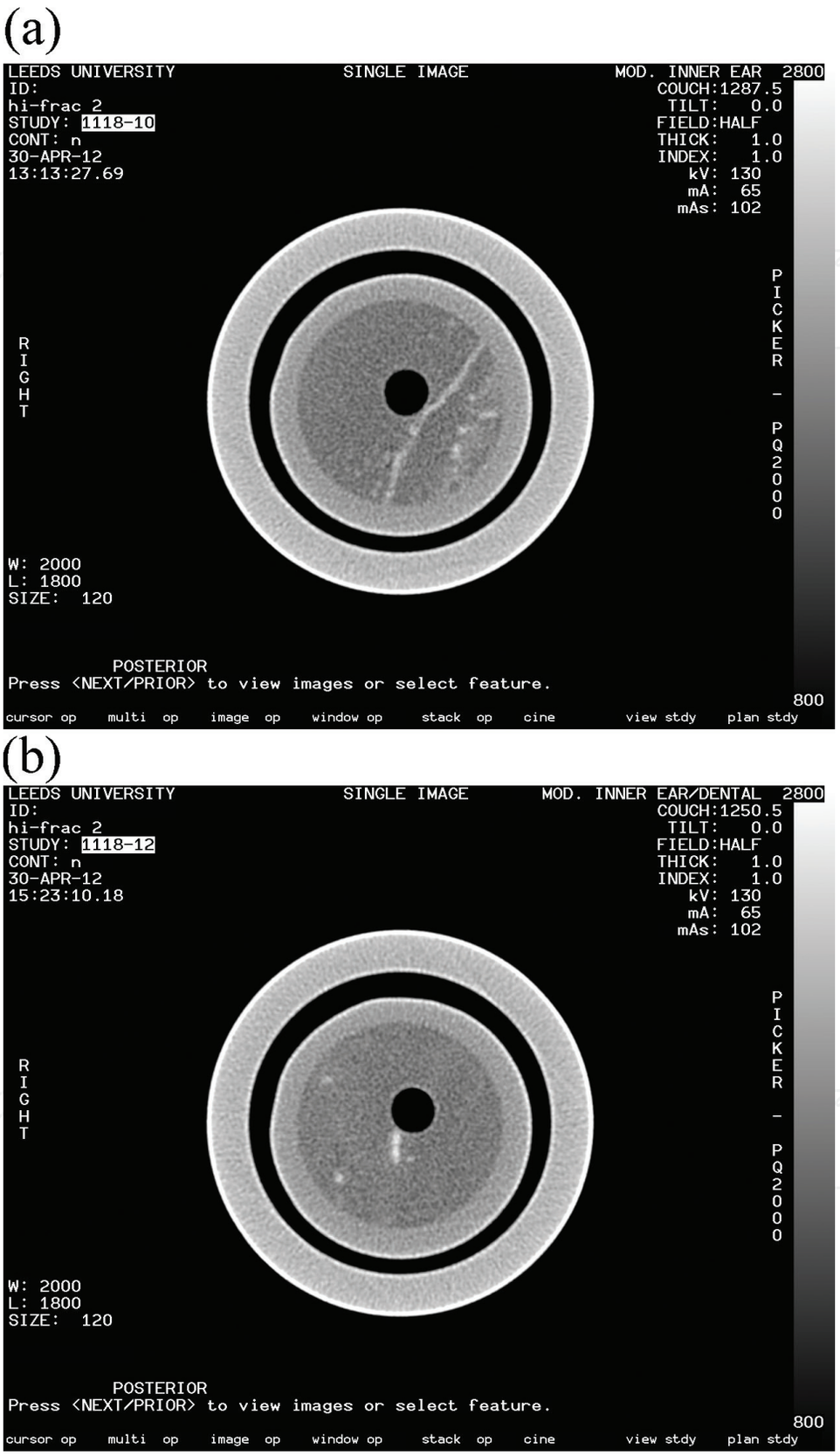

Figure 22. Scan images of the small cavity limestone specimen at different times during the fluid injection. (a) Early stage, (b) Later stage.

http://dx.doi.org/10.5772/intechopen.69732

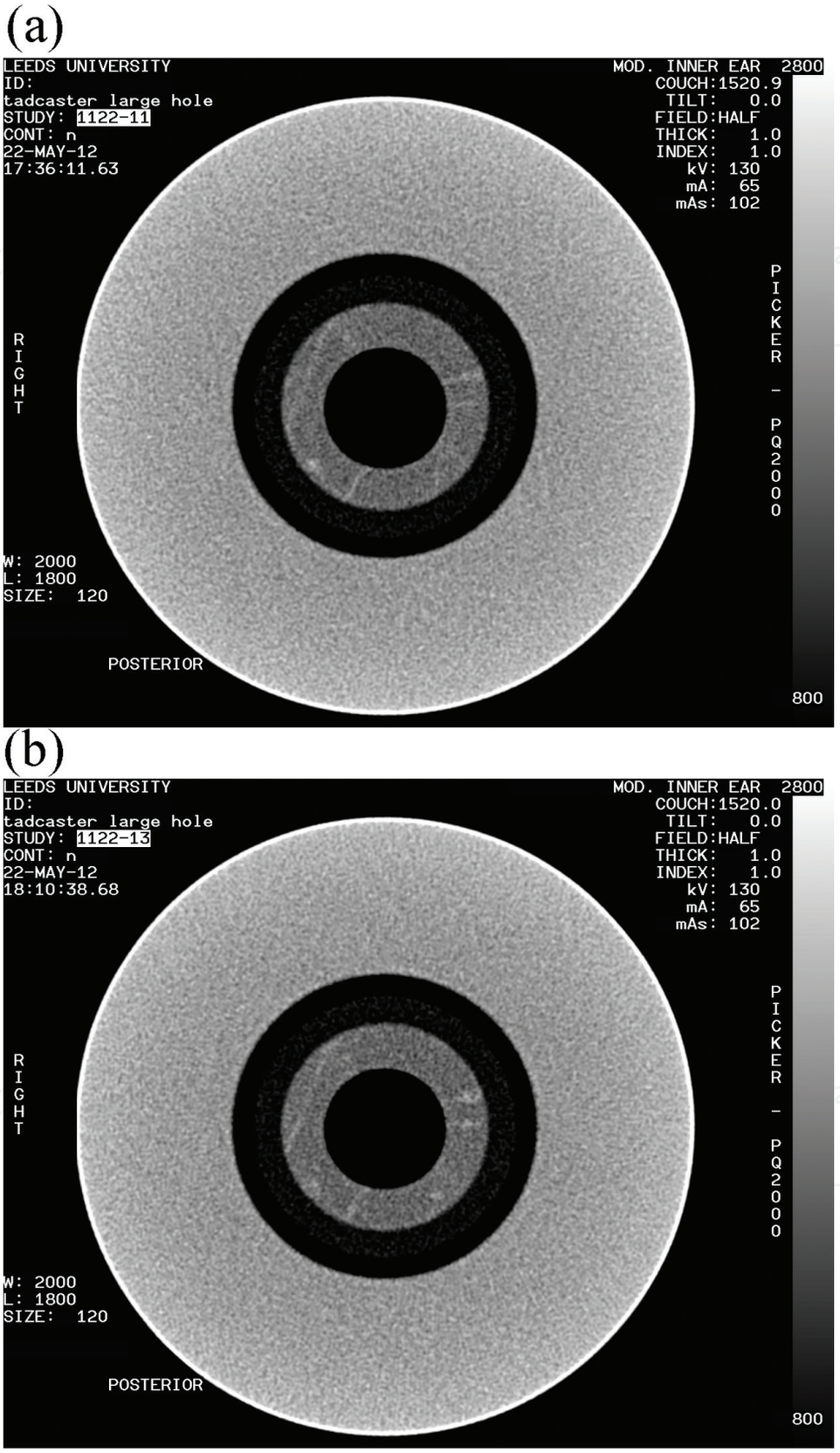

Figure 23. Scan images of the large cavity limestone specimen at different times before the initiation of fractures. (a) Early stage, (b) Later stage.

(13.79 MPa), creating a pressure gradient of 1000 Psi (6.9 MPa) over a period of 5 h (**Figure 24**). **Figure 22** depicts the outcome of the test. This was clearly not the case for the larger cavity specimen. Fluid pressure application on the larger cavity specimen was carried out by maintaining zero pressure at the cavity while increasing the magnitude of the outer boundary fluid pressure. Fracture initiation and the eventual collapse of the cavity wall occurred followed by a rapid drop in the circumferential pressure from 5056 to 29 Psi (34.86 to 0.2 MPa) (**Figure 25**). The initial state of the specimen and the progression in fracturing and collapse of the specimen is illustrated in **Figure 26**. The discrete element method (DEM) numerical simulation of

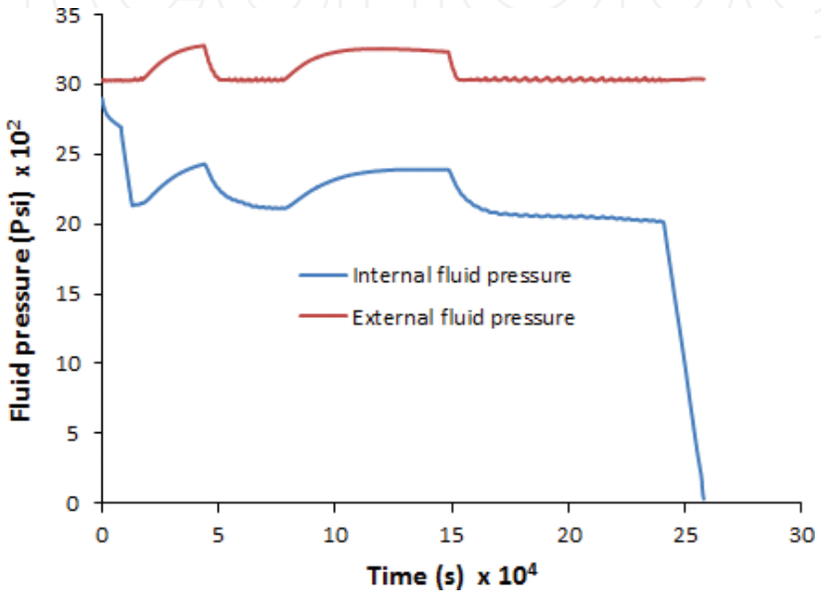

Figure 24. External and internal fluid pressure during injection (small cavity limestone specimen).

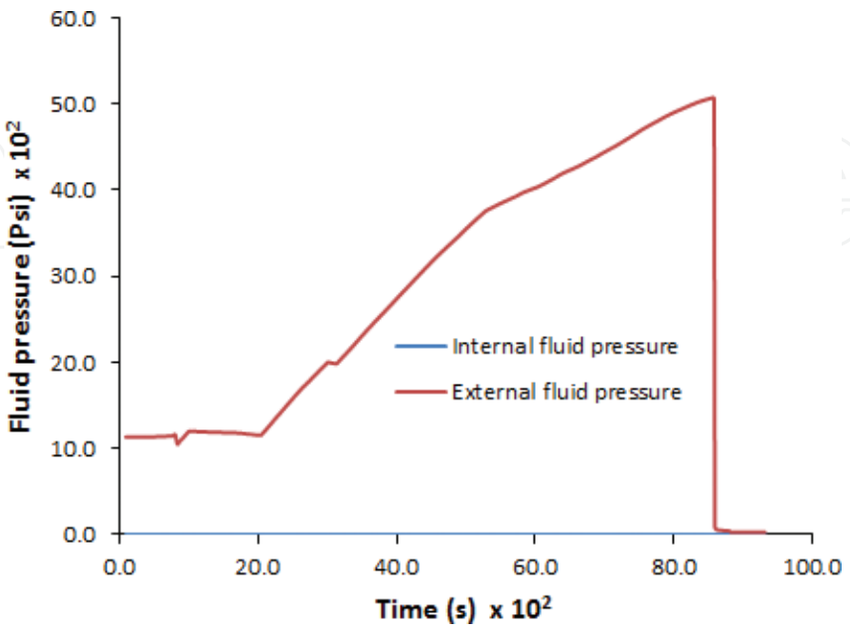

Figure 25. External and internal fluid pressure during injection (large cavity limestone specimen) [33].

http://dx.doi.org/10.5772/intechopen.69732

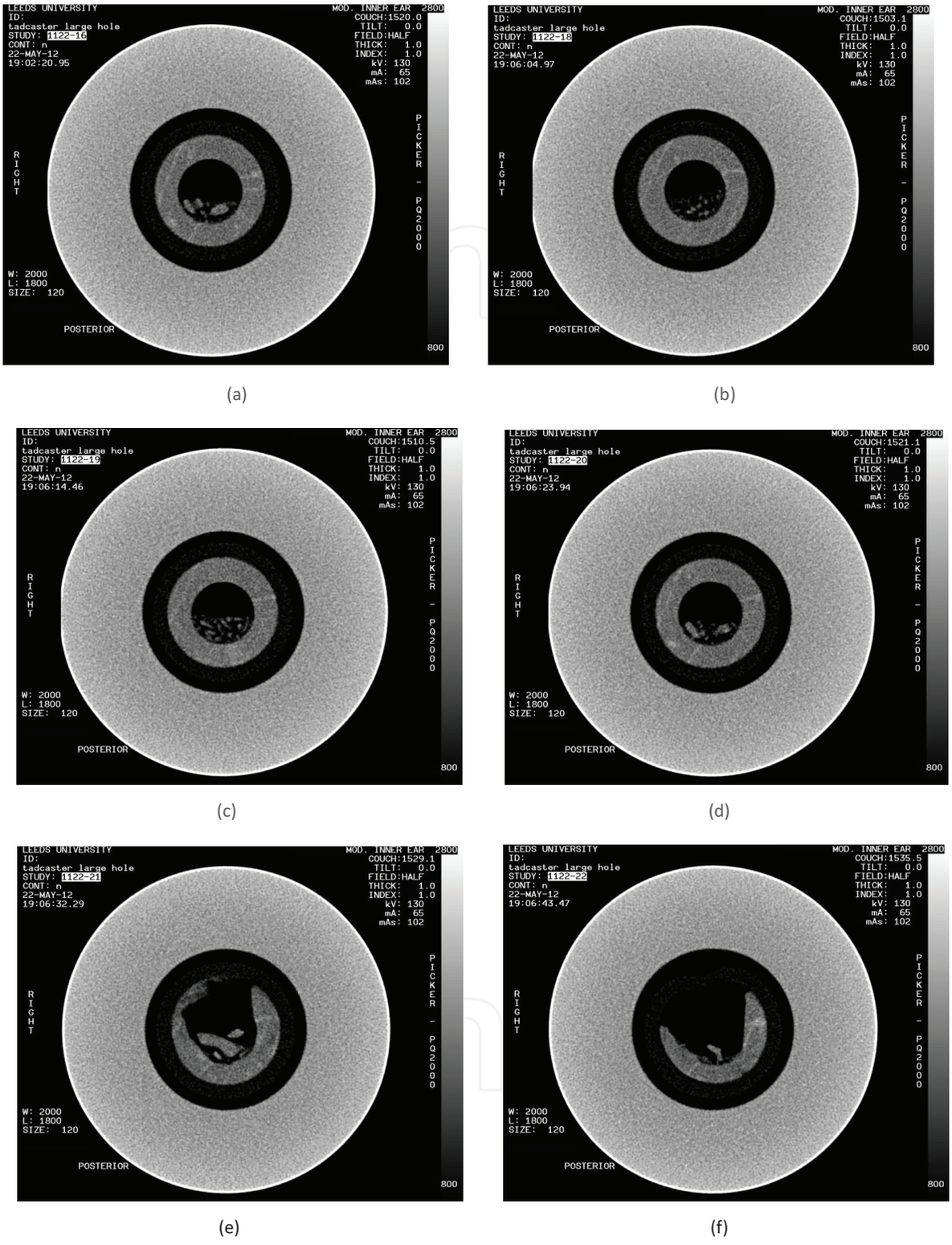

Figure 26. Scan images of the large cavity limestone specimen: fracture initiation and various times of collapse of the cavity wall. (a) Stage 1 (fracture initiation), (b) Stage 2, (c) Stage 3, (d) Stage 4, (e) Stage 5, (f) Stage 6.

this phenomenon is demonstrated in the work of Sousani et al. [33]. In these two cases, the difference in the mode of pressure loading does not significantly affect the behaviour of the specimen.

5. Summary remarks

Hydraulic fracturing experiments are often conducted at the laboratory scale involving miniature samples representative of outcrops or reservoir rocks. The set-up and implementation of these tests entail subjecting the rock specimen to initial and boundary conditions, as well as wellbore operating settings similar to those obtainable at the field scale. The accuracy of each set of tests is highly dependent on the propriety of design considerations and the application of influencing conditions. Six key elements are identified as crucial to the successful physical modelling of the hydraulic fracturing process. These are given as follows: specimen, *in-situ* stresses, pore pressure, fluid injection, duration, and visualisation and monitoring. It is crucial that the appropriate type of each element and/or combination of elements be adopted in order to truly reflect actual conditions.

Hydraulic fracturing experiments carried out on a variety of synthetic and natural rock samples illustrate a fracturing and collapse failure behaviour predominantly influenced by the material mechanical and physical properties, boundary conditions, as well as the mode of application of injection fluids. For soft rocks that are highly permeable, it is generally difficult to attain significant pressure build-up and the inward collapse of the cavity combined with a severe deformation of the material within the outer radius is imminent, occurring irrespective of the existence of a pressure gradient. Where the material strength and stiffness is increased, the maximum allowable build-up fluid pressure increases, the integrity of the outer radius away from the cavity is more likely to be maintained and the process of failure at the cavity is such that there is an initial expansion prior to the collapse of the cavity. The size of cavity plays a major role. Larger size cavities are considerably less stable than small cavities. Furthermore, where externally applied stresses are negligible, initiation and propagation of fractures will always occur perpendicularly to the axis of the cavity.

During the drilling of wells, it is suggested that considerations be given to the mechanical and physical properties of materials, especially at the immediate surroundings of wellbore. In addition, optimum well cavity sizes that would minimise the risk of failure and collapse should be determined.

Author details

Kenneth Imo-Imo Eshiet* and Yong Sheng

*Address all correspondence to: kenieshiet@yahoo.com

School of Civil Engineering, University of Leeds, Leeds, UK

References

[1] Ito T, Evans K, Kawaiand K, Hayashi K. Hydraulic fracture reopening pressure and the estimation of maximum horizontal stress. International Journal of Rock Mechanics and Mining Sciences. 1999;**36**(6):811-825

[2] Haimson B, Fairhurst C. Hydraulic fracturing and its potential for determining in-situ stresses a great depths. Transactions-American Geophysical Union. 1968;**49**(1):302

[3] Legarth B, Huengesand E, Zimmermann G. Hydraulic fracturing in a sedimentary geothermal reservoir: Results and implications. International Journal of Rock Mechanics and Mining Sciences. 2005;**42**(7-8):1028-1041

[4] Wan T, Sheng JJ. Enhanced recovery of crude oil from shale formations by gas injection in zipper-fractured horizontal wells. Journal Petroleum Science and Technology. 2015;**33**(17-18):1605-1610

[5] Zhang JC, Bian XB. Numerical simulation of hydraulic fracturing coalbed methane reservoir with independent fracture grid. Fuel. 2015;**143**:543-546

[6] Zhang J. Numerical simulation of hydraulic fracturing coalbed methane reservoir. Fuel. 2014;**136**:57-61

[7] King GE. Thirty years of gas shale fracturing: What have we learned? In: SPE Annual Technical Conference and Exhibition; 19-22 September; Florence, Italy. Society of Petroleum Engineers; 2010

[8] Hofmann H, Babadagliand T, Zimmermann G. Numerical simulation of complex fracture network development by hydraulic fracturing in naturally fractured ultra-tight formations. Journal of Energy Resource Technology. 2014;**136**(4):042907

[9] Middleton RS, Carey JW, Currier RP, Hyman JD, Kang Q, Karra S, Jimenez-Martinez J, Porterand ML, Viswanathan HS. Shale gas and non-aqueous fracturing fluids: Opportunities and challenges for supercritical CO_2. Applied Energy. 2015;**147**:500-509

[10] Deng JQ, Lin C, Yang Q, Liu YR, Taoand ZF, Duan HF. Investigation of directional hydraulic fracturing based on true tri-axial experiment and finite element modelling. Computers and Geotechnics. 2016;**75**:28-47

[11] Zhao Z, Guoand, J, Ma S. The experimental investigation of hydraulic fracture propagation characteristics in glutenite formation. Advances in Materials Science and Engineering. 2015;**2015**, Article ID 521480

[12] Zhou J, Chen M, Jinand Y, Zhang G-Q. Analysis of fracture propagation behaviour and fracture geometry using a tri-axial fracturing system in naturally fractured reservoirs. International Journal of Rock Mechanics & Mining Sciences. 2008;**45**:1143-1152

[13] Zhou J, Chenand M, Jin Y. Experimental investigation of hydraulic fracturing in random naturally fractured blocks. International Journal of Rock Mechanics & Mining Sciences. 2010;**47**:1193-1199

[14] de Pater CJ, Beugelsdijk LJL. Experiments and numerical simulation of hydraulic fracturing in naturally fractured rock. In: The 40th U.S. Symposium on Rock Mechanics (USRMS): Rock Mechanics for Energy, Mineral and Infrastructure Development in the Northern Regions. Anchorage, Alaska; 2005

[15] Beugelsdijk LJL, de Paterand CJ, Sato K. Experimental hydraulic fracture propagation in a multi-fractured medium. In: SPE Asia Pacific Conference on Integrated Modelling for Asset Management. Yokohama, Japan; 2000

[16] Guo J, Gouand B, Liu Y. Fracturing stimulations improve oil well performance in deep tight glutenite reservoirs of the Shengli oilfield. In: SPE Unconventional Resources Conference and Exhibition-Asia Pacific. Brisbane, Australia; 2013

[17] Alpern JS, Maroneand CJ, Elsworth D. Exploring the physicochemical processes that govern hydraulic fracture through laboratory experiments. In: The 46th US Rock Mechanics/Geomechanics Symposium. Chicago, IL, USA; 2012.

[18] Blanton TL. An experimental study of interaction between hydraulically induced and pre-existing fractures. In: Proceedings of SPE unconventional gas recovery symposium. Society of Petroleum Engineers; 1982.

[19] Wang Y, Fu H, Liang T, Wang X, Liu Y, Peng Y, Yangand L, Tian Z. Large-scale physical simulation experiment research for hydraulic fracturing in shale. In: SPE Middle East Oil and Gas Show and Conference. Manama, Bahrain; 2015

[20] Liberman M. Hydraulic Fracturing Experiments to Investigate Circulation Losses. M.Sc. Thesis. Missouri University of Science and Technology, Rolla, MO, USA; 2012

[21] Chen Z, Narayan SP, Yangand Z, Rahman SS. An experimental investigation of hydraulic behaviour of fractures and joints in granite rock. International Journal of Rock Mechanics & Mining Sciences. 2000;**37**:1061-1071

[22] Zoback MD, Rummel F, Jungand R, Raleigh CB. Laboratory hydraulic fracturing experiments in intact and pre-fractured rock. International Journal of Rock Mechanics and Mining Science & Geomechanics Abstracts. 1977;**14**(2):49-58

[23] Matsunaga I, Kobayashi H, Sasakiand S, Ishida T. Studying hydraulic fracturing mechanism by laboratory experiments with acoustic emission monitoring. International Journal of Rock Mechanics and Mining Sciences and Geomechanics Abstracts. 1993;**3**(7):909-912

[24] Brenne S, Molenda M, Stöckhertand F, Alber M. Hydraulic and sleeve fracturing laboratory experiments on 6 rock types. In: Bunger AP, McLennan J, Jeffrey R, editors. Effective and Sustainable Hydraulic Fracturing. InTech, Rijeka, Croatia; 2013

[25] Murdoch LC. Hydraulic fracturing of soil during laboratory experiments: Part 1. Methods and observation. Geotechnique. 1992;**43(2)**:255-265

[26] Murdoch LC. Hydraulic fracturing of soil during laboratory experiments Part 2. Propagation. Géotechnique. 1993;**43(2)**:267-276

[27] Murdoch LC. Hydraulic fracturing of soil during laboratory experiments Part 3. Theoretical analysis. Géotechnique. 1993;**43(2)**:277-287

[28] Ito T, Igarashiand A, Yamamoto K. Laboratory test of hydraulic fracturing in unconsolidated deformable rocks. In: Proceedings of the 4th Biot Conference on Poromechanics. New York; 2009. pp. 1001-1006.

[29] Omori Y, Jin S, Ito T, Naganoand Y, Sekine K. Experimental study of hydraulic fracturing in unconsolidated sands using X-ray CT method. In: The 47th US Rock Mechanics/Geomechanics Symposium. San Francisco, CA, USA; 2013

[30] Anderson E. The Dynamics of Faulting and Dyke Formation with Application to Britain. 2nd ed. Edinburgh: Oliver and Boyd; 1951

[31] Taherynia MH, Aghdaand SMF, Fahimifar A. In-situ stress state and tectonic regime in different depths of earth crust. Geotechnical and Geological Engineering. 2016;**34**679-687

[32] Molenda M, Stöckhert F, Brenneand S, Alber M. Acoustic emission monitoring of laboratory scale hydraulic fracturing experiments. The 49th US Rock Mechanics/Geomechanics Symposium; 28 June-1 July, 2015; San Francisco, CA, USA

[33] Sousani M, Eshiet KI-I, Ingham D, Pourkashanianand M, Sheng Y. Modelling of hydraulic fracturing process by coupled discrete element and fluid dynamic methods. Environmental Earth Sciences, 2014. **72(9)**:3383-3399

IntechOpen